Nonlinear deterministic sea wave prediction using instantaneous velocity profiles

Marion Huchet, Aurélien Babarit, Guillaume Ducrozet, Jean-Christophe Gilloteaux, Pierre Ferrant

Nonlinear deterministic sea wave prediction using instantaneous velocity profiles

Marion Huchet *, Aurélien Babarit, Guillaume Ducrozet, Jean-Christophe Gilloteaux, Pierre Ferrant

LHEEA, Centrale Nantes, 1 Rue de la Noë, 44 321, Nantes, CEDEX 3, France

Optimizing the production of wave energy converters using Model Predictive Control (MPC) requires a real-time, deterministic prediction of the waves arriving at the device. This study presents a new method for deterministic sea wave prediction, using the horizontal velocity profile over the water column as a boundary condition for a dedicated nonlinear wave model. However, direct measurement of the horizontal velocity component over the whole vertical column is hardly achievable at sea. A method to reconstruct this profile from measurement devices currently at use, such as ADCPs, is thus presented and evaluated. The performance of the prediction method itself is then tested using synthetic numerical data. First, the reconstruction of the horizontal velocity profile as a boundary condition is evaluated. Then, the whole prediction procedure is assessed. In both these stages, the simulations are based on synthetic numerical data and the outcomes are compared with numerical reference solutions. The results show that the method is promising enough to justify further investigation through wave tank experiments.

1. Introduction

While stochastic wave models such as WAM (The WAMDI Group, 1988), WAWEWATCH III (Tolman, 2009) or SWAN (Booij et al., 1999) are widely used today, e.g. in weather forecast or marine operation planning, they only provide statistical quantities on the sea state, such as significant wave height (H_s), peak period (T_p) or mean wave direction. Phase-resolved wave models, on the other hand, can offer a description of the actual shape of the sea surface. Such information, if available in real-time, would greatly benefit to a range of marine applications such as aircraft take-off and landing, ship dynamic positioning, or the development of control strategies for wave energy converters. For this latter application in particular, Model Predictive Control (MPC) appears to be a very promising method (Richter et al., 2013) that could increase the energy harvested by the device by up to 80% compared to regular Proportional Integral (PI) control (Nguyen et al., 2016). To be effective, a MPC strategy requires prior knowledge of the waves arriving at the device around 20 s ahead, advocating the need for an efficient, real-time, deterministic sea wave prediction tool.

Although they provide a detailed description of the sea surface, the high computational costs of phase-resolved wave models have long restricted their use to small time-space simulation domains. But recent progress in computational resources has revived interest in their development and they have emerged as a credible alternative for accurate, short-term wave prediction in the past 20 years (Morris et al., 1998). These deterministic wave models can classically be divided into linear and nonlinear methods. As frequently pointed out (Köllisch et al., 2018; Klein et al., 2020; Law et al., 2020), linear models benefit from a shorter computation time, a critical feature for real-time prediction, and are thus often preferred for operational purposes (Morris et al., 1998; Belmont et al., 2006; Naaijen and Huijsmans, 2008; Naaijen et al., 2009; Abusedra and Belmont, 2011; Kosleck, 2013; Naaijen et al., 2014b). They offer rather satisfying results for moderate sea states and short propagation distances, or for prediction requiring information on quiescent periods only (Belmont et al., 2014).

However, with increasing steepness of the sea state, nonlinear effects become significant and linear models fail to capture correctly the evolution of waves (Toffoli et al., 2008, 2010; Bonnefoy et al., 2010; Zhang et al., 2017). Following the early work of Zhang et al. (1999) who used a model truncated at second order in wave steepness, other weakly nonlinear approaches have then been developed for deterministic wave prediction. Accounting for nonlinearities up to the third order with a

* Corresponding author.
E-mail address: marion.huchet@ec-nantes.fr (M. Huchet).

narrow-band approximation, the Nonlinear Schrödinger equation (NLSE) framework is able to reproduce some nonlinear effects (Trulsen and Stansberg, 2001; Adcock et al., 2012; Simanesew et al., 2017). Trulsen (2005) conducted experimental validations of the NLSE method against laboratory measurements, for (among others) long-crested, irregular waves. Results showed that while the regular version of the NLSE brings little to no benefits compared to the linear theory, the modified version of the equation (MNLSE, enhanced with exact linear dispersion), on the other hand, greatly improves the wave modelling. Additionally, Simanesew et al. (2017) compared various versions of the Schrödinger Equation with linear models and provided an analysis on short-crested waves prediction. They stressed out that when too little information is available on the directionality of incoming waves, nonlinear models do not perform better than linear ones and the lack of reliable input data represents a more constraining blocking point than the propagation step itself.

Among higher-order models, the HOS method (Wu et al., 2000; Wu, 2004; Blondel et al., 2010; Blondel-Couprie et al., 2013; Köllisch et al., 2018; Klein et al., 2019) has proved to be particularly promising for nonlinear wave prediction on large space-time domains (Wu, 2004; Blondel et al., 2010) thanks to its high numerical efficiency and accuracy, even for short-crested waves, and has thus been chosen for this study.

When using a HOS method with operational applications in mind, the main difficulty does not lie in the propagation step itself, but in initializing the model from field measurements (Köllisch et al., 2018; Fucile et al., 2018). Most of the computational time is actually spent in processing the wave data collected with the technology available at sea, in order to provide a valid initial condition: this pre-processing step today represents the main obstacle to real-time prediction (Blondel et al., 2010; Köllisch et al., 2018). Much of the work conducted to overcome this challenge has focused on extracting wave information from sea surface elevation data, either through the use of wave buoys or radar imaging (Blondel et al., 2010; Naaijen et al., 2014b). However, to properly initialize a conventional HOS model, a snapshot of the sea surface elevation is not sufficient and additional independent information is required: classically, the velocity potential at the free surface.

As this is not a piece of information easily retrievable from field measurements, this quantity can either be approximated at first order (Klein et al., 2019) or computed with a data assimilation scheme (Aragh and Nwogu, 2008; Blondel-Couprie and Naaijen, 2012; Yoon et al., 2016; Köllisch et al., 2018), none of these methods being fully satisfying because of the approximations or additional computational cost induced.

The present article thus proposes a different, innovative approach, based on wave-induced fluid velocity data instead of sea surface elevation data. Information on the incoming sea state is collected in the form of instantaneous vertical profiles of the horizontal velocity over the whole water column, at one fixed location upstream the point of interest. This data is used as a boundary condition in a propagation model, which then provides a wave prediction at the point of interest. The propagation model used is the open-source, nonlinear potential code HOS-NWT. It is based on the pseudo-spectral High-Order Spectral (HOS) method (Dommermuth and Yue, 1987; West et al., 1987) and has been developed at Centrale Nantes (Ducrozet et al., 2006, 2012). The HOS-NWT model was designed to model a numerical wave tank and was slightly adapted here to fit for ocean wave prediction purposes. The core of the propagation method remains unchanged with regards to the original HOS methods, but the boundary and initial conditions differ, allowing nonlinear wave prediction without depending on the initialization of the spatial free surface quantities, which are difficult to retrieve from field data. As the HOS-NWT model itself is already widely validated (Bonnefoy et al., 2010; Ducrozet et al., 2006, 2012), the propagation part of the prediction procedure does not raise any particular difficulty, as long as the underlying hypotheses are met. Hence, the challenge lies in determining a suitable boundary condition from the velocity data collected upstream, in the water column.

As it turns out, direct access to instantaneous, horizontal velocity profiles is not achievable with the measurement technologies currently available. However, reconstructing such information from measurements acquired with an ADCP (Acoustic Doppler Current Profiler) seems within reach (Huchet et al., 2018).

This paper presents a numerical assessment of this new prediction method. The ability to produce a good quality boundary condition from velocity data retrievable with the available measurement technologies is evaluated, as well as the quality of the wave prediction obtained. The numerical verification is conducted on uni-directional irregular waves, using synthetic measurement data.

2. Propagation - prediction method

2.1. Hypotheses

This study is carried out in 2D (uni-directional waves only), ignoring wind forcing, with a finite, constant water depth h and with no ambient currents. The considered space domain $\mathscr{D}$ has horizontal bounds set at $x = x_0$ and $x = x_0 + L_x$ and vertical bounds delimited by the flat bottom at $z = -h$ and the free surface position at $z = \eta(x,t)$. It is associated with a Cartesian coordinate system (O,x,z). Its origin O is set at one corner of the domain, with (Ox) representing the horizontal axis (waves propagating towards $x > 0$) and (Oz) the vertical one, oriented upwards, with $z = 0$ set at the mean water level at rest (see Fig. 1).

We assume that the hypotheses underlying the use of potential flow theory are valid: the fluid is considered inviscid and incompressible and the flow is irrotational. Wave breaking is not accounted for here and $z = \eta(x,t)$ describes the free surface position in the space-time domain.

Finally, this work was conducted using synthetic numerical data, meaning that the results discussed in section 3 do not take into account measurement errors such as instrument bias or noise. In the following sections, if encountered the term “measurements” will thus refer to synthetic data generated with a reference numerical model.

2.2. General outline

The method developed here aims at providing an accurate wave prediction over a horizon of a few wave periods (30–60 s), using a fixed velocity measurement device located upstream the area of interest. The adopted approach, illustrated in Fig. 1, consists in measuring the instantaneous wave-induced velocity in the water column, at a fixed position x_0. The collected data is used to recover the profile of the horizontal component of fluid velocity at x_0: $U(x_0,z,t)$. This horizontal velocity profile is then passed on as a boundary condition in the deterministic wave model HOS-NWT, which generates and propagates the corresponding waves downstream, to the area of interest. The proposed prediction methodology considers the fluid at rest as initial conditions, the waves being generated from the boundary condition at $x = x_0$. The method then runs in two steps: first, the reconstruction of the sea state, then the prediction itself.

- The reconstruction phase, of duration T and arbitrarily set in the past in this study, relies on continuously updated velocity measurements. For $-T \leq t \leq 0$, the velocity data collected at coordinate x_0 in the water column is used by the HOS-NWT model, via its boundary condition, to generate and propagate the corresponding waves downstream, as illustrated in Fig. 1a.
- In the second step ($t > 0$) illustrated in Fig. 1b, data on the incident waves at x_0 is not updated anymore and the boundary condition is set to zero in HOS-NWT. Therefore, the model only propagates information collected before $t = 0$. This marks the beginning of the prediction phase itself.

This method allows to model nonlinear, irregular sea states

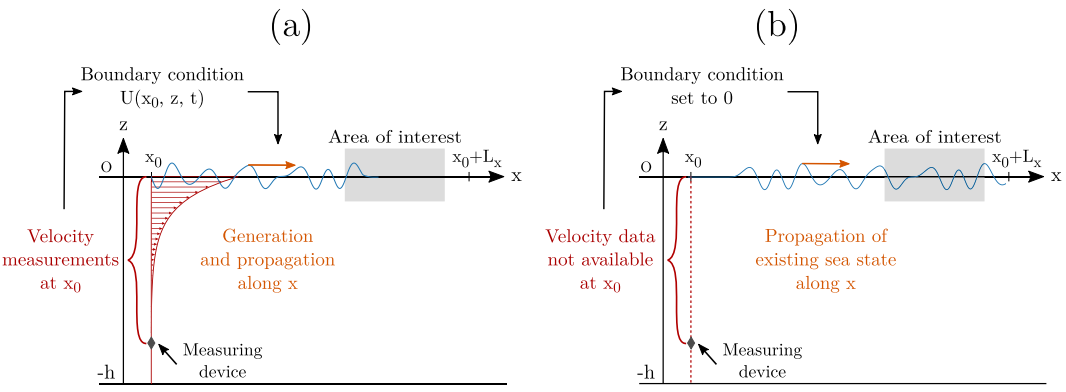

Fig. 1. General method. (a) Wave generation and propagation; (b) Wave prediction.

accurately. More importantly, contrary to many other wave models, it does not rely on any data assimilation step to provide the surfacic initial conditions usually required, resulting in a substantial improvement in computation time. The particular steps of reconstructing the boundary condition and propagating the waves are detailed below, as well as the need to define correctly the region where an accurate prediction is theoretically available.

2.3. Theoretical prediction zone

As the information collected on the incoming sea state is limited in time and space, so is the region where a reliable deterministic wave prediction can be achieved. The predictable zone $\mathscr{D}_{x,t}$ is then defined as the space-time domain accessible to deterministic sea wave prediction from the available measurements. Several publications have already extensively addressed the definition of this predictable zone for various measurement configurations (Wu, 2004; Naaijen et al., 2014a; Qi et al., 2018b; Fucile et al., 2018), hence only the broad lines for our simplified uni-directional case are reminded here.

A 2D (uni-directional), irregular wave field being continuously measured by a fixed-point device located at $x = x_0$ can be represented by its wave power spectral density, as in Fig. 2. a. Assuming that the energy content of this spectrum is negligible outside some frequency bounds f_{min} and f_{max} judiciously set, the sea surface elevation at a given point (x_1, t_1) can be correctly predicted only if all relevant frequency components (between f_{min} and f_{max}):

- were measured at x_0 between $t = -T$ and $t = 0$;
- were propagated to x_1 between $t = -T$ and $t = t_1$.

The predictable zone is then bounded by the propagation of both the slowest component, measured at $t = -T$, and the fastest component, measured at $t = 0$, as illustrated in Fig. 2b.

These bounds translate into limiting group velocities $C_{g_{min}}$ and $C_{g_{max}}$, which are evaluated here using the linear dispersion relation: although the waves considered in this article are nonlinear, studies have shown that the predictable region defined assuming a linear sea state is actually more restrictive than when taking nonlinearities into account, so the linear definition gives a minimal estimation of the prediction zone (Wu, 2004; Blondel-Couprie, 2009; Qi et al., 2018a). $C_{g_{min}}$ and $C_{g_{max}}$ in turn depend on the choice of the frequency bounds f_{min} and f_{max}, which must represent the wave spectrum as accurately as possible while assuring a sufficient prediction horizon. Here, following Blondel et al. (2010) (but unlike Wu (2004)), f_{min} and f_{max} are defined so as to retain only components with an energy density which is at least 5% of the one at the peak of the wave spectrum, as illustrated in Fig. 2a.

For the considered space-time domain where $x \geq x_0$ and $t \geq -T$, the predictable zone is then defined by the following double inequality (Blondel-Couprie, 2009):

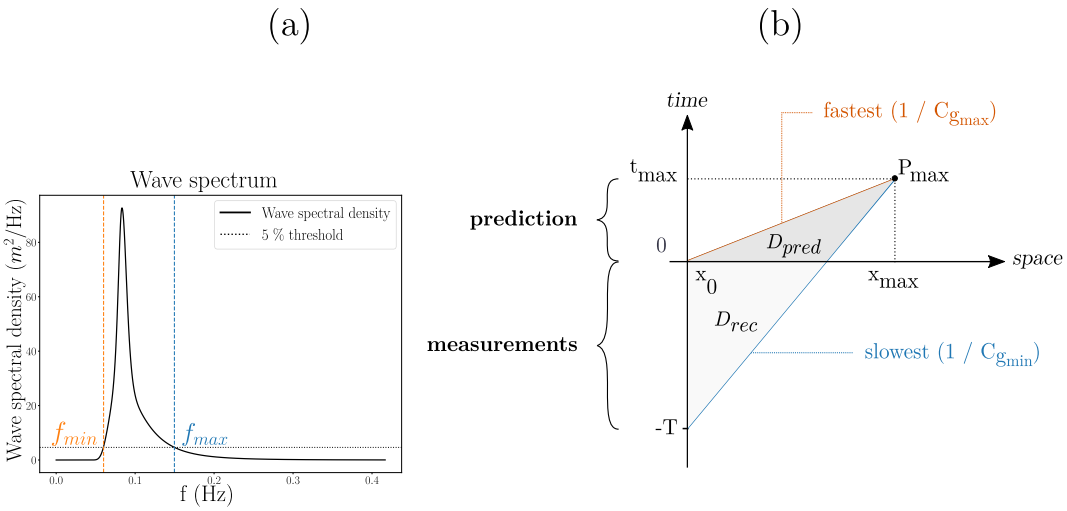

Fig. 2. Definition of the theoretical zone $\mathscr{D}_{x,t}$ accessible to deterministic prediction from a single fixed measuring device, set at x_0 and collecting data for $t \in [\ -T\ ;\ 0\ ]$. (a) f_{min} and f_{max} are defined by cutting off wave components accounting for less than 5% of wave energy density at the peak; (b) The prediction zone $\mathscr{D}_{x,t}$ depends on measurement duration T and group speeds considered: $C_{g_{min}}$ and $C_{g_{max}}$. It can be further subdivided into a hindcast zone $\mathscr{D}_{rec}$ (in light grey) and a forecast zone $\mathscr{D}_{pred}$ (in darker grey).

$$(x_1,t_1)\in\mathscr{D}_{x,t} \quad \text{if} \quad \frac{x_1-x_0}{C_{g_{min}}}\leq t_1\leq T+\frac{x_1-x_0}{C_{g_{max}}} \tag{1}$$

and bounded by points (x_{min},t_{min}) and (x_{max},t_{max}), of coordinates:

$$\begin{cases} x_{min}=x_0, \quad x_{max}=x_0+T\dfrac{C_{g_{min}}.C_{g_{max}}}{C_{g_{max}}-C_{g_{min}}} \\ t_{min}=-T, \quad t_{max}=T\dfrac{C_{g_{min}}}{C_{g_{max}}-C_{g_{min}}} \end{cases} \tag{2}$$

t_{max} being the maximum time prediction horizon. It is represented in Fig. 2b. As already stressed in paragraph 2.2, the predictable zone $\mathscr{D}_{x,t}$ is actually made up of two subregions: a "hindcast" zone, labelled $\mathscr{D}_{rec}$ on Fig. 2b for $t\in[\,-T\,;\,0\,]$, and the zone where actual prediction takes place, labelled $\mathscr{D}_{pred}$, for $t\in[\,0\,;\,t_{max}\,]$.

Wave predictions obtained through the use of a single, fixed measurement device are considered valid only within the predictable region defined above. Hence, when evaluating the methodology presented in this work, the error on the free surface elevation prediction will be calculated only in this zone. This restriction does not apply to the results of the horizontal velocity reconstruction, as this is not a prediction step.

2.4. *Reconstruction of the boundary condition from wave data*

The first requirement for wave prediction is to retrieve information on the incoming sea state from field measurements, to feed the propagation model. In the method developed here, the data is needed in the form of instantaneous horizontal velocity profiles along the water column. Unfortunately, due to practical constraints, this kind of information is not accessible today: no measuring technology is yet able to provide a full horizontal velocity profile with a single instrument. To tackle this problem and because the method was developed from the outset with practical applicability in mind, a benchmarking study on the velocity measurement technologies currently available was carried out (Huchet, 2017). From this work, it appeared that only one type of measurement device was likely to provide instantaneous data on velocity in the whole water column, while limiting the number of instruments deployed (associated to higher costs): acoustic Doppler current profilers (ADCPs). These instruments rely on the Doppler effect to measure the velocity of small suspended particles in the water, which are assumed to have the same speed as the fluid itself. ADPCs are often installed with an up-looking, bottom-mounted configuration. They usually present 4 diverging beams with an angle of $20-30°$ to the instrument's axis and measure radial velocity profiles for each beam, the distance between the volumes of water sensed by each beam increasing with the distance to the instrument. Traditional post-processing methods reconstruct the 3D mean velocity components from these radial velocities, using trigonometric relations. This reconstruction is based on the assumption that "the statistical properties of the flow are horizontally homogeneous" (Lu and Lueck, 1999), meaning that at a given depth, the velocities measured by the four diverging beams (at different horizontal coordinates) present the same *mean* amplitude and direction at the time scales considered. When measuring mean currents, this is a reasonable hypothesis and the method has proved its worth over the years. In the case of deterministic wave measurements however, relying on the statistical horizontal homogeneity of velocities is not useful, because we are interested in instantaneous, single-ping velocity measurements rather than in time-averaged quantities. Other methods were specifically developed for wave measurements from ADCP data (Terray et al., 1999; Nortek, 2017), but they still rely on time-averaged quantities. Therefore, they can only provide phase-averaged information, such as mean wave direction or significant wave height. This is not relevant for the present application and a new dedicated method is then needed to recover deterministic useable data from available ADCP measurements.

Beside the classical four divergent beams, some recent ADCP models are also equipped with a fifth vertical one, allowing to retrieve a well-resolved profile of the vertical velocity component (Nortek, 2017). The present paragraph then proposes a method to reconstruct an instantaneous horizontal velocity profile using the vertical beam of two ADCPs (the other four beams being de-activated to avoid interference).

With the configuration illustrated in Fig. 3, the two ADCPs are separated by a distance Δx in the direction of wave propagation and measure instantaneous vertical velocity profiles noted: $W\left(x_0\pm\frac{\Delta x}{2},z,t\right)$.

The assumption of irrotational flow previously stated in paragraph 2.1: $\nabla\times\mathbf{v}=0$ *in* $\mathscr{D}$ can also be written:

$$\partial_z U(x,z,t)=\partial_x W(x,z,t) \quad in \quad \mathscr{D}, \tag{3}$$

with $\mathbf{v}=(U,W)$ the fluid velocity, U and W its horizontal and vertical components in the Cartesian coordinates system previously defined, and ∂_x and ∂_z the partial derivatives with respect to x and z. At any given time, the instantaneous reconstructed horizontal velocity profile $\widehat{U}$, at x_0 and at an arbitrary depth z_0, can then be expressed as:

$$\widehat{U}(x_0,z_0,t)=\int_{z_{ref}}^{z_0}\partial_x W(x_0,z,t)\,dz+U\left(x_0,z_{ref},t\right) \tag{4}$$

where z_{ref} is an arbitrary reference depth for which horizontal velocity data $U(x_0,z_{ref},t)$ is available. Assuming vertical velocity measurements are available over the whole water column at $x=x_0\pm\frac{\Delta x}{2}$ (for example through the use of ADCPs) and provided Δx is small enough and measurements are synchronized in time, the instantaneous horizontal derivative for W at given space coordinates can be estimated with:

$$\begin{aligned}\partial_x W(x_0,z_0,t) &=\frac{1}{\Delta x}\left[W\left(x_0+\frac{\Delta x}{2},z_0,t\right)-W\left(x_0-\frac{\Delta x}{2},z_0,t\right)\right]+O(\Delta x^2)\\ &=\frac{\Delta W(x_0,z_0,t)}{\Delta x}+O(\Delta x^2)\end{aligned} \tag{5}$$

with $\Delta W(x_0,z_0,t)=W\left(x_0+\frac{\Delta x}{2},z_0,t\right)-W\left(x_0-\frac{\Delta x}{2},z_0,t\right)$. A classical integration scheme with a composite trapezoidal rule leads to the following approximated expression for $\widehat{U}(x_0,z_0,t)$:

$$\begin{aligned}\widehat{U}(x_0,z_0,t) =&\frac{1}{\Delta x}\sum_{k=1}^{N_z}\frac{\Delta W(x_0,z_{k-1},t)+\Delta W(x_0,z_k,t)}{2}\Delta z_k+U\left(x_0,z_{ref},t\right)\\ &+O(\Delta x^2)+O(\Delta z^2)\end{aligned} \tag{6}$$

with z_k the integration grid points dividing the interval $[z_{ref};z_0]$ into N_z subintervals of respective length Δz_k, with no *a priori* requirement for a

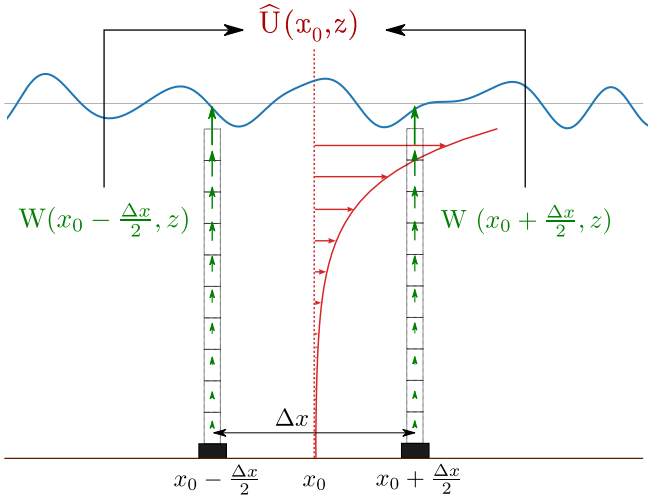

Fig. 3. Reconstruction method for U, using data collected from two vertical velocity profiles.

uniform grid. Here, Δz_k correspond to the sizes of the measuring cells for the ADCPs.

For deep water applications and assuming the vertical velocity profile W is measured until velocity is negligible, $U(x_0, z_{ref})$ can be set to zero. In intermediate water depth, a local measuring device should be added, to provide a reference horizontal velocity. In this study, we assume that the vertical velocity profiles are measured in the whole water column and that the reference velocity $U(x_0, -h)$ is known.

With this procedure, which presently assumes perfect measurements (no bias, no noise, etc.), the quality of the reconstruction depends mainly on: i) the quality of the approximation made for the partial derivative $\partial_x W$, with a theoretical accuracy in $O(\Delta x^2)$; ii) the vertical discretization of vertical velocity profiles, responsible for the integration error on z varying in $O(\Delta z^2)$; and iii) the accurate knowledge of the horizontal velocity at $z = z_{ref}$. As the method relies on instantaneous data, the quality of the reconstruction does not depend on the time discretization of vertical velocity data.

It should be noted that this reconstruction method, here written for uni-directional sea states, can be extended to short-crested waves configurations: additional measurement devices located at $\left(x_0, y_0 \pm \frac{\Delta y}{2}\right)$ could provide an estimation of $\partial_y W(x_0, y_0, z, t)$, allowing to deduce the horizontal velocity along y: $V(x_0, y_0, z, t)$. It is also worth mentioning in this critical assessment that the method is expected to be less accurate in the case of a flow with vorticity as well as in the presence of currents, because the underlying equation $\nabla \times v = 0$ is not valid anymore.

2.5. Wave propagation model: HOS-NWT

The second part of the prediction method concerns the propagation of the kinematics known at a fixed location. Once the incoming sea state has been measured at x_0, it is used as a boundary condition to generate and propagate the waves along (Ox) thanks to the open-source HOS-NWT model,[1] a nonlinear, deterministic Numerical Wave Tank based on the HOS method. It was chosen because of its capabilities to model a wavemaker and the induced wave generation and propagation accurately and efficiently (Ducrozet et al., 2012) and has been slightly adapted to fit our prediction purpose. The generation of waves through a wavemaker is indeed very similar to the target application of generating waves by imposing a velocity profile at a fixed location. The very good numerical performance of the model and its high level of accuracy make it a particularly suitable tool for predicting complex, nonlinear sea states while retaining the possibility of real-time applications.

The present section summarizes the main features of the model and the minor changes made for the purposes of this study. It is adapted from Ducrozet et al. (2006) and additional information on the original HOS-NWT model may be found there. Here, we consider the fluid domain $\mathscr{D}$ previously defined, with horizontal dimension L_x and finite depth h. The section $x = x_0$ originally corresponds to the wavemaker's rest position while the section $x = x_0 + L_x$ represents a perfectly reflective wall. Under the potential flow hypotheses introduced in paragraph 2.1, the continuity equation: $div\vec{V} = 0$ leads to the Laplace equation for the velocity potential φ: $\Delta\varphi = 0$ in the fluid domain $\mathscr{D}$. The bottom boundary condition is expressed in the form of a no-flow condition: $\partial_z\varphi = 0$ at $z = -h$. Then, following Zakharov (1968), the free surface boundary conditions are written in a fully-nonlinear form and using surface quantities, namely the free surface elevation η and the surface potential $\varphi^S(x,t) = \varphi(x, z = \eta, t)$:

$$\partial_t\eta = \left(1 + |\nabla\eta|^2\right)\partial_z\varphi - \nabla\varphi^S.\nabla\eta \tag{7}$$

$$\partial_t\varphi^S = -g\eta - \frac{1}{2}\left|\nabla\varphi^S\right|^2 + \frac{1}{2}\left(1 + |\nabla\eta|^2\right)(\partial_z\varphi)^2 \tag{8}$$

on $z = \eta(x,t)$. With this formulation, the only remaining non-surfacic quantity is the vertical velocity at the free surface: $W = \partial_z\varphi(x, z = \eta, t)$. This term is evaluated using the order-consistent High-Order Spectral (HOS) method of West et al. (1987), which allows a rapid and accurate resolution of the free surface equations at an arbitrary order of nonlinearity M. This primary expression of the free surface boundary conditions is common to both the original HOS formulation, developed for open domains (Dommermuth and Yue, 1987; West et al., 1987; Ducrozet et al., 2007; Bonnefoy et al., 2010), and to its adapted version for numerical wave tanks used in this article.

The main difference between the original and the NWT formulations results from the lateral boundary conditions: instead of imposing periodic conditions on $x = x_0$ and $x = x_0 + L_x$, in the HOS-NWT model these boundary conditions are expressed as homogeneous Neumann conditions (no-flow conditions). The basis functions used for the spectral representation of the velocity potential are modified accordingly and become the natural modes of the closed wave tank.

Originally in the HOS-NWT model, the boundary reflecting the presence of the wavemaker ($x = x_0$ at rest) is modelled by a no-flow condition, imposed between $z = -h$ and $z = 0$ at the position X of the wavemaker:

$$\partial_x\varphi(x,z,t) = \partial_t X(z,t) + (\partial_z X(z,t)).(\partial_z\varphi(x,z,t)) \quad \text{at} \quad x = X(z,t). \tag{9}$$

As this boundary condition is not directly taken into account by the spectral formulation, further developments are necessary to be able to impose the exact wavemaker boundary condition. The potential φ, solution of the total problem, is then separated into two components, following Agnon and Bingham (1999): $\varphi = \varphi_{spec} + \varphi_{add}$, where φ_{spec} is the spectral potential describing the evolution of the free surface in a fixed-geometry tank (with a no-flow condition on $x = x_0$) and φ_{add} is the additional potential accounting for the presence of the wavemaker and satisfying Equation (9).More details may be found in Bonnefoy et al. (2010) and Ducrozet et al. (2012).

In the modified version of the model implemented here, the decomposition into φ_{spec} and φ_{add} remains but the no-flow condition at the wavemaker's position is simplified into a horizontal velocity profile, corresponding to the wave-induced kinematics, directly imposed at x_0:

$$\partial_x\varphi(x,z,t) = U(x,z,t) \quad \text{at} \quad x = x_0, \tag{10}$$

with U being the instantaneous, full-depth horizontal velocity profile that could be obtained via on-site measurements. Compared to the original version of HOS-NWT, this modification has the advantage of applying the last boundary condition directly at $x = x_0$ and of removing the difficulties to account for a moving boundary, since the potential gradient $\partial_x\varphi$ is directly available.

Finally, it can be noted that the reflective wall at $x = x_0 + L_x$ is preceded by an absorbing zone in the numerical model, reproducing the beach present near the end wall of most physical wave tanks to absorb the incoming energy. Its implementation in the model is done through a local modification of the free-surface dynamic boundary condition and is not detailed here, but can be found in Bonnefoy et al. (2006). This is useful to our application as well, as it prevents wave reflections, provided the simulation domain is set long enough (i.e., L_x must be large enough) for the absorbing zone not to overlap with the prediction area.

Compared to conventional HOS methods based on periodic open boundaries, this new version adapted from a numerical wave tank is particularly interesting for prediction applications. Indeed, here the model does not require any initialization step based on the knowledge of two independent spatial quantities: η and φ^S, the latter being hardly deducible from field data. Instead, the waves are continuously generated through the boundary condition at x_0 using velocity data, which should be more easily available with existing measurement techniques. The

[1] Code available at: https://github.com/LHEEA/HOS-NWT.

associated wave prediction is expected to be accurate even for nonlinear sea states. The following section aims at evaluating this statement through numerical experiments.

3. Numerical assessment using 2D synthetic wave fields

In this section, we present the process followed to numerically assess the potential of the prediction method previously developed. First, the reconstruction of the boundary condition using vertical velocity profiles is evaluated, then the wave generation and prediction phase is also tested. In both steps, we use synthetic numerical data as a reference for comparison, meaning that measurement errors are not taken into account in the final prediction error.

3.1. Wave cases studied and reference data

The wave cases studied were chosen with the same characteristics as in Wu (2004), in order to allow comparison on prediction performances. Generated in infinite water depth, they are characterized by a uni-directional JONSWAP spectrum with a peak enhancement factor $\gamma = 3.3$ and a peak period $T_p = 12s$, from which the peak wavelength λ_p is deduced by the dispersion relation. For each wave case, the significant wave height and its corresponding wave steepness, defined as $\varepsilon_c = H_s/\lambda_p$, are reported in Table 1.

The synthetic sea states used as reference data were generated using another open-source nonlinear wave model, HOS-ocean[2] (Ducrozet et al., 2016). This reference model is based on the original, open-sea HOS method with periodic horizontal boundary conditions. The method is widely used to study large-scale and long-time propagation of nonlinear sea states and is assumed to be an accurate representation of the real sea conditions (Ducrozet et al., 2007; Toffoli et al., 2010; Xiao et al., 2013; Sergeeva and Slunyaev, 2013).

The numerical parameters for the simulations were selected in order to ensure converged results: $k_{max}/k_p \approx 16$ and the tolerance threshold was 10^{-7} for the time-stepping process. To be consistent with Wu's test cases, the reference data sets were generated with an order of HOS expansion $M = 4$. Additionally, for each sea state considered, $N_{sim} = 100$ different phase sets were simulated to ensure the statistical convergence of the results (Monte Carlo simulations).

Each run provided 51 T_p of simulation, from which only $41T_p$ were actually available for comparison. Indeed, the simulations were initialized with a linear wave field (through a JONSWAP spectrum and a set of random phases), which is known to create risks of numerical instabilities. To avoid this, the initialization procedure described in Dommermuth (2000) was implemented, introducing a transition period of duration $T_a = 10\ T_p$ during which a relaxation scheme was applied on the nonlinear terms in the free surface boundary conditions (Equation (7) and (8)). This allowed a smooth transition from a linear initial condition to a fully nonlinear wave field, which could then be considered realistic. After this transition period, the remaining $41T_p$ of actually useable data were divided into:

- 30 T_p of hindcast, for which the boundary condition provided at x_0 by the reference model was updated in time;
- 11 T_p of prediction, for which the boundary condition was set to zero.

In addition to the surfacic information classically made available by such models, in these reference simulations the velocities were also evaluated inside the fluid domain, thanks to a dedicated method (Ducrozet et al., 2005; Choi et al., 2017). The reference data sets hence provided fields of sea surface elevation: $\eta(x,t)$, as well as horizontal and vertical velocities $U(x,z,t)$ and $W(x,\ z,\ t)$, available in the whole space-time domain.

Table 1
Characteristics of the sea states studied. JONSWAP spectrum, $T_p = 12s$ and $\gamma = 3.3$.

H_s **(m)**	0.48	3.75	6.26	7.82
$\varepsilon_c = H_s/\lambda_p$ **(%)**	0.2	1.7	2.8	3.5

3.2. Reconstruction of the horizontal velocity profile

This section is dedicated to the numerical verification of the method, introduced in section 2.4, to reconstruct the horizontal velocity profile $\widehat{U}(x_0,z,t)$ used as a boundary condition in our propagation model HOS-NWT. Here, the synthetic numerical data described in 3.1 are used both as an input data base ($W(x_0 \pm \Delta x/2, z, t)$) to feed the reconstruction method and as reference results ($U(x_0,z,t)$) for the assessment of the present method.

The reconstruction of the boundary condition is needed only in the "hindcast" phase of the general prediction method, hence this step is applied only for $t \in [-T; 0]$. The velocity reconstruction is evaluated on the sea states described in Table 1. It is assumed that the horizontal velocity at z_{ref} introduced in Equation (4), needed as additional information, is known (here, $z_{ref} = -h$). The distance between the measuring devices is set to an ideally small value: $\Delta x = 3.5m \approx \lambda_p/64$. The vertical velocity profiles are also supposedly measured along a very fine grid: $\Delta z = 0.55m \approx \lambda_p/410$, in order to minimize the integration error.

As the method relies only on instantaneous velocity data from adjacent locations, the quality of the reconstruction is independent from the time stepping used, provided the measurement devices are correctly synchronized in time. (The updating rate of the boundary condition could influence the quality of generation and propagation of the waves; but this aspect is independent of how well a single velocity profile is reconstructed). Hence, each reconstruction at a given time step is independent from the others and the duration of the simulation taken into account is the only relevant time parameter here to provide a consolidated view on the results. To ensure statistical convergence, for each wave case the velocity reconstruction is then computed on the whole "hindcast" phase of duration T, for all the $N_{sim} = 100$ simulations with different phase sets. Performance assessment is conducted using statistical indicators such as the bias on velocity *amplitudes* $b_{|U|}(z)$ and the normalized, root-mean-square error $NRMSE_U(z)$:

$$b_{|U|}(z) = \frac{1}{N_{sim}} \sum_{i=1}^{N_{sim}} \frac{1}{T} \int_{-T}^{0} \left| \widehat{U}_i(x_0,z,t) \right| - |U_i(x_0,z,t)|\ dt \tag{11}$$

$$NRMSE_U(z) = \sqrt{\frac{\sum_{i=1}^{N_{sim}} \int_{-T}^{0} \left[\widehat{U}_i(x_0,z,t) - U_i(x_0,z,t) \right]^2 dt}{\sum_{i=1}^{N_{sim}} \int_{-T}^{0} U_i(x_0,z,t)^2\ dt}} \tag{12}$$

where:

- $i = 1, \ldots, N_{sim}$ is the realization index;
- T is the duration of the hindcast phase; here, $T = 30\ T_p$;
- U_i is the reference horizontal velocity profile for the ith random phase set;
- $\widehat{U_i}$ is the corresponding velocity profile reconstructed using Equation (4).

[2] Code available at: https://github.com/LHEEA/HOS-ocean.

As illustrated in Fig. 4, for all sea cases studied, the bias on amplitudes is negative: the method tends to slightly under-estimate the amplitudes (both positive and negative) of the reconstructed velocity, especially near the sea surface. However, even in the worst sea case considered here, the bias on amplitudes remains below 1.5 cm s^{-1} at $z = 0$, representing $\approx 1.1\%$ of the root-mean-squared velocity at this depth for the corresponding sea state. The bias being a dimensional quantity, as expected it increases with wave steepness, since for a given value of T_p, the velocities themselves increase with H_s. Regarding the NRMS error, plotted in Fig. 5, a common thread to all sea states is that its magnitude depends on depth and increases significantly close to the free surface. The figure also brings out a dependency on the sea state considered: for the lowest steepnesses, the error remains very low (under 4%) throughout the whole profile, whereas for more severe sea states the shape of the error profile is modified and the error near the sea surface undergoes a noticeable increase, up to 14% in the worst case. However, the NRMS error is a quadratic indicator and even a rather high value can correspond to quite satisfying results, as shown in Fig. 6: the reference and reconstructed velocity time series are plotted for $z = 0$. At this depth, these quantities do not always have a physical meaning and rather represent extrapolated values, because when a wave trough passes over x_0 the fluid velocity does not exist at $z = 0$; but the corresponding data is still needed as part of the boundary condition for HOS-NWT, which is defined for $z \in [-h; 0]$. The time series are plotted for a single realization, on a subrange of time steps for which the NRMS error matches the converged value: Fig. 6 then illustrates that a NRMS error of 14% actually allows an accurate reconstruction of the velocity time series.

An alternative way of visualizing the results is proposed in Fig. 7. The probability density function of the absolute error, normalized by the RMS reference velocity, is plotted at $z = 0$ (the same precautions as in Fig. 6 apply as to its physical meaning). As can be seen in the figure, the vast majority of errors remains below 10% for the three first sea states studied. The last sea state ($H_s = 7.82m$), exhibiting the highest degree of nonlinearity, shows a wider distribution curve, but the errors stay at very reasonable levels.

The results presented above were obtained through a numerical verification, conducted for various sea states and stabilized over many realizations. They give a first insight into the method's ability to reconstruct a suitable instantaneous horizontal velocity profile, from synthetic data mimicking the operation of devices that were not primarily designed for deterministic wave measurements. Of course, these results need to be consolidated with experiments, taking into account more realistic measurement configurations (cell size, spacing between devices) as well as measurement errors; but these preliminary findings allow to extend the numerical study to wave prediction using this reconstructed velocity profile as a boundary condition. This is the topic of the next section.

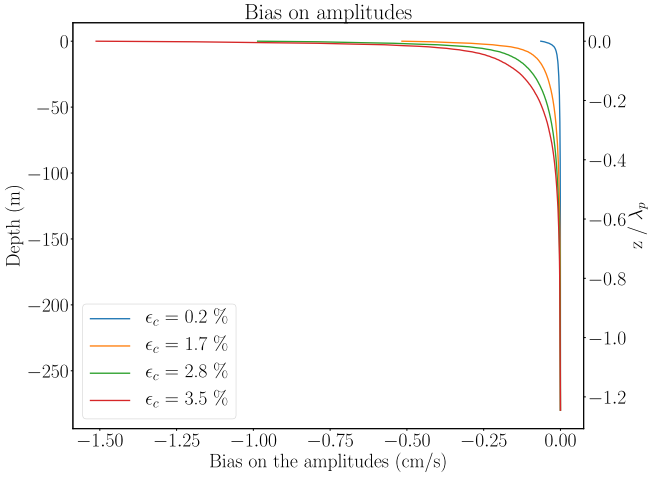

Fig. 4. Bias on the amplitudes of reconstructed horizontal velocity, as a function of depth (right y-axis is depth normalized by peak wavelength). Results are presented for the wave steepnesses ϵ_c listed in Table 1.

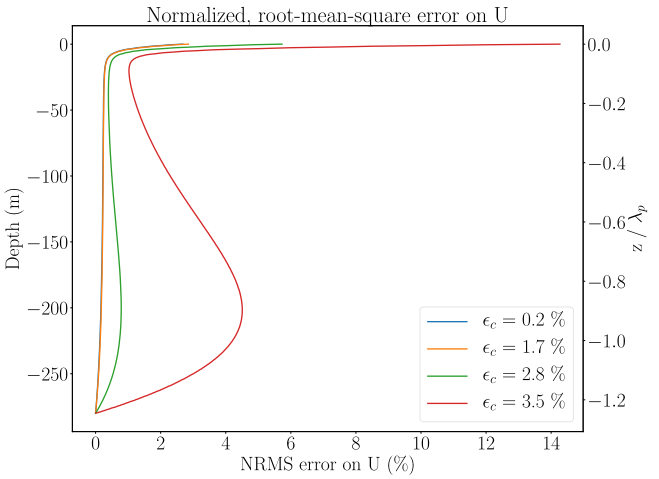

Fig. 5. NRMS error on the reconstructed horizontal velocity, as a function of depth (right y-axis is depth normalized by peak wavelength). Results are presented for the wave steepnesses ϵ_c listed in Table 1.

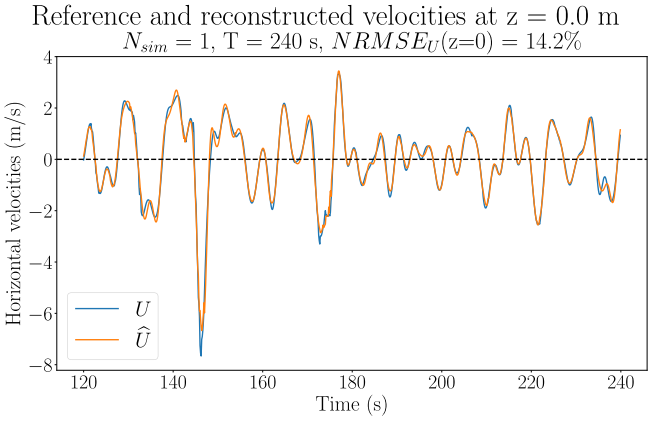

Fig. 6. Extract of a reconstructed velocity time series at $z = 0$ for $\epsilon_c = 3.5\%$ ($H_s = 7.82m$). The NRMS error on U computed on these 240 s is comparable to the converged error value. Hence, the time series is a good illustration of what can be expected in terms of velocity reconstruction.

3.3. *Propagation and prediction*

In this section, a numerical verification is conducted on the prediction method. The wave prediction is computed using the reconstructed horizontal velocity profile $\widehat{U}(x_0, z, t)$ as a boundary condition in the propagation model HOS-NWT. Although the reference data sets were generated in infinite water depth (as stated in section 3.1), in HOS-NWT depth must be set to a finite value and was thus chosen large enough for the velocities to be near zero at the bottom: $h = 280m$, when the dispersion relation gives $\lambda_p \approx 225m$. The numerical parameters were selected in order to ensure convergence of the results. The k_{max}/k_p ratio ranged between 25 and 32 according to the sea state considered and for all cases, the tolerance parameter for the time integration was set to 10^{-6} and the order of nonlinearity for HOS-NWT simulations to $M = 5$.

The quality of the prediction is evaluated by calculating the error on $\eta(x, t)$, using the same indicators as in Wu (2004). A field of RMS error, normalized by significant wave height, is first defined as:

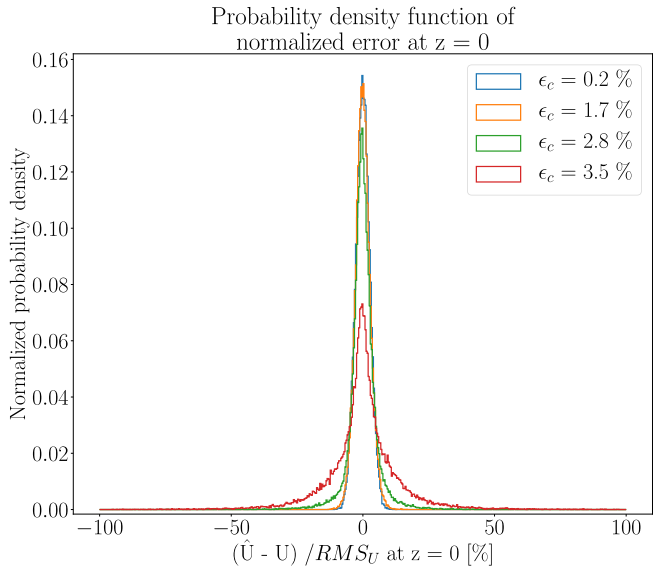

Fig. 7. Distribution of error on the reconstructed velocity, as a percentage of the RMS reference velocity, at $z = 0$. Results are presented for the different wave steepnesses ε_c listed in Table 1.

$$\varepsilon(x,t) = \sqrt{\frac{\sum_{i=1}^{N_{sim}} \left[\eta^i_{pred}(x,t) - \eta^i_{ref}(x,t)\right]^2}{N_{sim}}} \times \frac{2}{H_s} \tag{13}$$

with $N_{sim} = 100$ being the number of Monte Carlo simulations computed to ensure statistical convergence of the results, η_{ref} the output of the reference simulations and η_{pred} the output of the prediction method. The corresponding maps of the normalized prediction error are presented in Fig. 8 for all sea states considered.

The white solid lines mark out the prediction zone as defined in section 2.3. The white dashed line divides it further into hindcast and prediction sub-areas. Here the frequency f_{min} and f_{max}, used to compute the relevant group velocities, were chosen so as to cut off wave frequencies accounting for less than 5% of the wave energy at the spectrum's peak. As can be seen in Fig. 8, the prediction zone is a good indicator of where the wave prediction can be considered relevant, with a clear error minimization in the area defined as predictable, for all sea states considered. In the prediction zone, the error (averaged on 100 runs) remains below 15% even for large wave steepness and even stays below 10% up to a moderately high steepness of $\varepsilon_c = 2.8\%$, which compares well with the results of Wu (2004). The figure also shows that the error increases with the nonlinearity of the sea states. Yet the propagation part of the HOS-NWT model is already well validated, even for highly nonlinear cases, hence this increase in error is probably due to an unsatisfactory implementation of the boundary condition at x_0. This assumption is supported by the observation that the error also increases with x and t in the propagation direction of the waves, which is especially visible in the most energetic sea case.

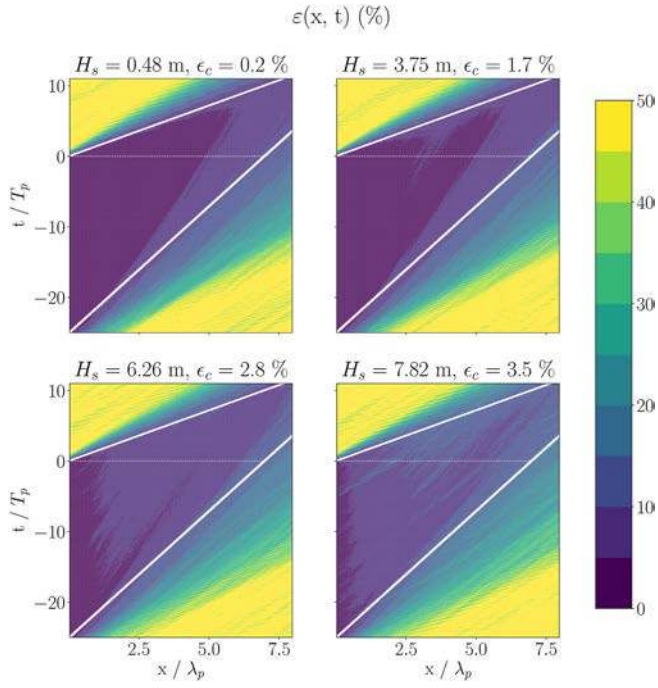

Fig. 8. Error $\varepsilon(x,t)$, calculated from Eq. (13) using 100 phase sets for each sea state listed in Table 1. The solid white lines materialize the bounds of the theoretical prediction zone $\mathscr{D}_{x,t}$. The horizontal, dotted white line divides it into reconstruction and prediction sub-regions.

Beside the error maps, a more synthetic indicator is also used, averaging the previous error $\varepsilon(x,t)$ in the prediction zone and resulting in a single scalar error per sea state:

$$\varepsilon^{\mathscr{D}} = \frac{\iint_{\mathscr{D}_{x,t}} \varepsilon(x,t)\,dx\,dt}{\iint_{\mathscr{D}_{x,t}} dx\,dt} \tag{14}$$

where $\mathscr{D}_{x,t}$ stands for the theoretical prediction zone. This mean error is reported in Table 2, along with the errors obtained by Wu (2004) and Blondel et al. (2010) with the same formula.[3]

The results show a similar prediction quality for Wu, Blondel and the new method presented here. Even the case with a wave steepness $\varepsilon_c = 3.5\%$ is quite satisfying, considering our reconstructed velocity presents a NRMS error of about 14% near the sea surface. Besides, as our prediction method does not require any data assimilation to initialize the propagation model, these results represent a significant improvement in terms of computational efficiency while providing a prediction as accurate as that obtained with other nonlinear methods.

The error indicators presented above are useful to compare our results with previous attempts on deterministic prediction. However, they lack information on the nature of this error because they do not discriminate between amplitude and phase errors. Yet, the latter is particularly important to model predictive control for wave energy converters, since it is crucial to know exactly when each wave will arrive at the device. A complementary error quantity is thus proposed here: the normalized cross-correlation between the reference signal and the predicted one, allowing to evaluate the similarity between two time series. At a given x_C coordinate, the cross-correlation factor C is expressed as a function of the time shift τ between the two signals:

Table 2
Prediction errors averaged on the whole prediction zone, for wave fields with varying steepness, and from: (a) Wu (2004); (b) Blondel et al. (2010); the present prediction method using $\hat{U}$.

H_s (m)	ε_c (%) $= H_s/\lambda_p$	$\varepsilon^{\mathscr{D}}$ (%) from (a)	$\varepsilon^{\mathscr{D}}$ (%) from (b)	$\varepsilon^{\mathscr{D}}$ (%) present
0.48	0.2	5.25	5.3	4.14
3.75	1.7	5.53	5.7	4.87
6.26	2.8	5.07	6.4	6.74
7.82	3.5	8.19	8.9	9.19

[3] The numerical values for Blondel et al. (2010) were estimated from their Figure 13.

$$C(\tau) = \frac{1}{t_{max} - t_{min}} \int_{t_{min}}^{t_{max}} \frac{\eta_{pred}(x_C,\ t)}{\sigma_{pred}} \times \frac{\eta_{ref}(x_C, t+\tau)}{\sigma_{ref}} dt \tag{15}$$

where $\sigma_{ref} = std(\eta_{ref}(x_C,\ t_{min} \leq t \leq t_{max})$ is the standard deviation of η_{ref} in the prediction zone (the same applies to σ_{pred}) and $t_{min,max}$ are the bounds of the theoretical prediction zone at the specific coordinate x_C considered. From this cross-correlation function, the maximum value $max(C)$ and its corresponding time shift T_s are extracted as indicators of how well the signal is reconstructed at point x_C: $max(C)$ assesses how well the shape and amplitude of the predicted signal match the reference one, and T_s indicates the time delay for which signals are best aligned with one another. As an example, two identical signals with no time shift between them will show $max(C) = 1$ and corresponding $T_s = 0s$.

For a given sea state and phase set, these two quantities $max(C)$ and T_s are calculated at each point x_C of the simulation domain, assessing the evolution of the prediction's quality over space. The calculations use data from dedicated simulations, run with a refined sampling rate to identify more accurately a potential phase shift. For each sea state in Table 1, $max(C)$ and T_s are computed separately for 25 different phase sets then ensemble-averaged, allowing to present converged results. The results are plotted in Fig. 9 as a function of a "dimensionless fetch", expressed as $\chi = \varepsilon_c^2 k_p x$. This quantity, adapted from Trulsen and Stansberg (2001) (save a π multiplication factor), corresponds to the propagation distance scaled by the steepness squared. It allows displaying results for different sea states on the same graphs and looking for general trends, assuming the important nonlinear physical processes at play scale accordingly. This applies for example to nonlinear modulation or nonlinear (phase) velocities.

This Fig. 9 presents a comparison between linear and nonlinear prediction capabilities: starting from the same information provided by the velocity boundary condition $\widehat{U}(x_0,z,t)$, the wave propagation part of the method is computed both for linear ($M = 1$) and nonlinear ($M = 5$) HOS-NWT simulations. The objective here is to assess the influence of nonlinearities during wave propagation, all procedures being strictly equivalent otherwise.

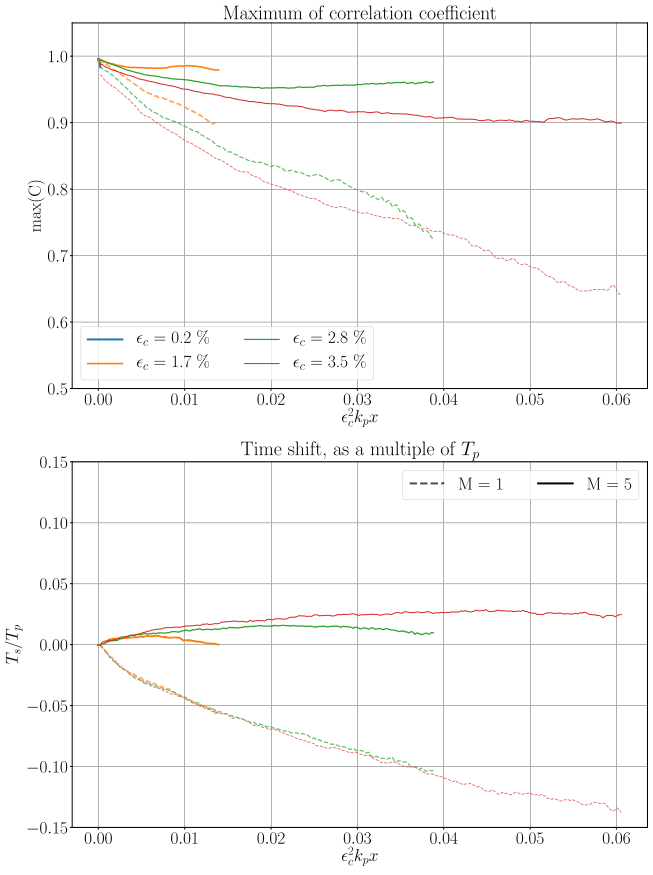

Fig. 9. Correlation results plotted against the fetch scaled by the square of the steepness: $\chi = \varepsilon_c^2 k_p x$. (a). Correlation factor. (b) Phase shift. Dotted lines correspond to linear predictions, solid lines of the same thickness to their equivalents in nonlinear prediction with M = 5.

Because the steepness associated to $H_s = 0.48m$ is small, the scaled fetch is too, and results for this sea state are hardly readable on Fig. 9. A dedicated plot would show that for this case, as expected the prediction quality is very similar for linear and nonlinear simulations. However this is true only for a very small steepness (or equivalently, short dimensionless fetch).

The other sea states considered highlight diverging results between linear and nonlinear predictions as the scaled fetch increases. Even though the cross-correlation is computed in the prediction zone only, the quality of linear prediction deteriorates rapidly. Results show a decline in amplitudes similarity as well as the appearance of a phase shift. The most noticeable feature is that linear prediction fails to maintain correct phase information, even after a relatively short distance, and that the increase of the error is driven by the dimensionless fetch χ, as the evolution of phase shift shows perfect agreement from one sea state to another. Discarding the influence of the different y-intercepts, this scaling is also relevant for the correlation factor $max(C)$, which reaches low values for the largest scaled fetch considered here. This evolution was expected, as both nonlinear phase velocity effects and nonlinear amplitude modulation are known to scale with ε_c^2 (Zakharov, 1968; Longuet-Higgins and Phillips, 1962; Trulsen, 2005).

Nonlinear prediction, on the other hand, offers a good prediction quality both in terms of correlation magnitude and of phase shift. The nonlinear method shows a decrease in the correlation coefficient for short scaled fetch. With increasing propagation distance, it stabilizes at different values depending on the sea states, the worst-case level being around 0.9 for the highest steepness considered. This is a far more satisfying result than their linear equivalent and a good performance in itself, as will be seen shortly with Fig. 10. The method also proves able to deliver a reliable phase information for all cases considered. The different curves do not overlap as much as for the linear predictions, but their evolutions are similar and altogether the phase shift remains within less than 5% of T_p.

The common behaviour observed for linear simulations of different sea states confirms that when nonlinearity is not taken into account, the error evolves with the steepness squared. The disappearance of this

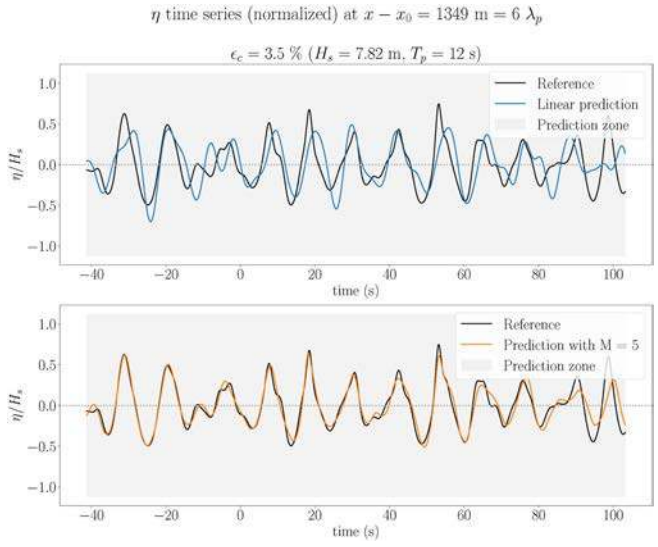

Fig. 10. Sea surface elevation time series, normalized by H_s, at $x = x_0 + 6\lambda_p$ for $\varepsilon_c = 3.5\%$ ($\chi = 0.5$).

scaling in the nonlinear results confirms that the predominant nonlinear effects are well taken into account by the HOS method, as expected. The remaining dispersion of the results according to the steepness considered, however, suggest that other sources of error should be looked for. Higher-order nonlinear effects in the wave propagation are a first possibility. The error made on the boundary condition at x_0 is also a likely candidate here, as it was shown in section 3.2 that the quality of the reconstructed velocity depended on the steepness considered.

The very good performance of the nonlinear method in maintaining the phase information over long distances is finally illustrated in Fig. 10.

It displays time series of η, for both linear and nonlinear predictions, at $\chi = 0.5$. This corresponds to the sea state with the largest steepness ($\varepsilon_c = 3.5\%$, $H_s = 7.82m$) captured at $x = 6\lambda_p$ from the "measurement" point at x_0. The error $\varepsilon^{\mathscr{D}}$ associated to this specific realization (hence, "averaged" on 1 run only) is 10.8%, a value slightly superior to the error averaged on 100 runs reported in Table 2 and the corresponding correlation factor is 0.95, a little better than the mean value in Fig. 9. Fig. 10 highlights the difference in prediction quality between linear and nonlinear wave propagation, as well as the ability of the proposed method to deliver a suitable prediction tens of seconds ahead, even for highly nonlinear sea states. As this improvement is mainly due to a correct calculation of the phase velocity, which takes non-linearities into account, it would be worth investigating the performance of other methods such as weakly nonlinear wave models: they could be faster than HOS while retaining a correct phase velocity. The "Choppy Wave" Model (Nouguier et al., 2009) would be an interesting candidate, especially its improved second-order formulation proposed by Desmars et al. (2018) which introduces corrections for the phase and group velocities accounting for some nonlinearities.

4. Conclusion

A new deterministic wave prediction method was proposed in this article, using instantaneous velocity profile measurements as input data for a wave propagation model based on a HOS method. This allows to model even highly nonlinear sea states accurately, a feature which is non negligible in the time and space scales considered here. An important aspect of the method is the reconstruction, from field data, of the horizontal velocity profile used as a boundary condition in the propagation model. A pre-processing step was developed to ensure the recovery of useable information from the type of *in situ* velocity measurements actually available nowadays: here, ADCP data were judged the most suitable candidate. The velocity reconstruction, then the wave prediction process were evaluated numerically, using uni-directional synthetic sea states and assuming an ideal measurement configuration: no measurement error, a small distance between the instruments and a very large number of measurement points in the water column.

The reconstructed velocity profiles were compared to reference time series and the method proved able to provide a reliable boundary condition to the propagation model, even though for the steepest wave case, the quality of the reconstruction is slightly less satisfying close to the free surface. The whole prediction process was then evaluated numerically. We used the same test cases and error indicators as previous studies on deterministic wave prediction based on the HOS method, to compare our results with the state of the art. Our approach provided a similar prediction quality while dispensing with the step of data assimilation necessary for other methods, which should greatly reduce the required computing time. The interest of using a nonlinear propagation model was confirmed using cross-correlation indicators, to compare the amplitude and phase errors between linear and nonlinear predictions. It showed evidence that for the space and time scales considered, our method provides far superior results than one based on a linear propagation model. Presenting the evolution of error along a propagation distance scaled by the steepness squared highlighted some common behaviours for linear predictions, and further quality deterioration with increasing distance or steepness can be extrapolated for these simulations. On the contrary, nonlinear prediction results do not scale with this parameter while retaining some variability from one steepness to another. As the propagation method used is known to correctly manage the third-order nonlinear effects at play with the ε_c^2 scaling, the remaining differences could be attributed to higher order effects in the propagation and to errors in the reconstruction of the boundary condition at x_0. Generalization to any arbitrary sea state remains risky, but from the available results one could expect the method to maintain satisfying phase information for any steepness considered, while the amplitude and shape accuracy (given by the correlation factor) is likely to deteriorate with increasing steepness.

Finally, as stated above, in this article the velocity reconstruction was computed assuming an ideal "measurement" configuration. Additional tests, not presented here, have analyzed the sensitivity of this reconstruction to measurement configuration; several measurement parameters were modified, such as the spacing between instruments, the ADCP cell size or the availability of data close to the free surface. As could be expected, this sensitivity study showed a loss of quality for the velocity reconstruction when numerical tests mimicked a more realistic measurement configuration. However, the prediction obtained from this less accurate boundary condition remained good enough to justify conducting an experimental validation of the method in the wave basin of Centrale Nantes. The results will be presented in a future paper.

CRediT authorship contribution statement

Marion Huchet: Conceptualization, Methodology, Software, Data curation, Validation, Formal analysis, Writing - original draft, Visualization. **Aurélien Babarit:** Conceptualization, Methodology, Writing - review & editing, Supervision, Project administration, Funding acquisition. **Guillaume Ducrozet:** Conceptualization, Methodology, Software, Data curation, Writing - review & editing, Supervision. **Jean-Christophe Gilloteaux:** Conceptualization, Methodology, Writing - review & editing, Supervision. **Pierre Ferrant:** Conceptualization, Methodology, Writing - review & editing, Supervision.

Declaration of competing interest

The authors declare that they have no known competing financial interests or personal relationships that could have appeared to influence the work reported in this paper.

Acknowledgments

This work is supported by the Agence de la transition écologique (ADEME).

References

Abusedra, L., Belmont, M.R., 2011. Prediction diagrams for deterministic sea wave prediction and the introduction of the data extension prediction method. Int. Shipbuild. Prog. 58 (1), 59–81 publisher: IOS Press. URL. https://content.iospress.com/articles/international-shipbuilding-progress/isp69.

Adcock, T.A.A., Gibbs, R.H., Taylor, P.H., 2012. The nonlinear evolution and approximate scaling of directionally spread wave groups on deep water. Proc. Math. Phys. Eng. Sci. 468 (2145), 2704–2721. URL. https://royalsocietypublishing.org/doi/full/10.1098/rspa.2012.0029.

Agnon, Y., Bingham, H.B., May 1999. A non-periodic spectral method with application to nonlinear water waves. Eur. J. Mech. B Fluid 18 (3), 527–534. URL. http://www.sciencedirect.com/science/article/pii/S0997754699800478.

Aragh, S., Nwogu, O., 2008. Variation assimilating of synthetic radar data into a pseudo-spectral wave model. J. Coast Res. 2008 (10052), 235–244 publisher: Coastal Education and Research Foundation. URL. https://bioone.org/journals/journal-of-coastal-research/volume-2008/issue-10052/1551-5036-52.sp1.235/Variation-Assimilating-of-Synthetic-Radar-Data-into-a-Pseudo-spectral/10.2112/1551-5036-52.sp1.235.full.

Belmont, M.R., Christmas, J., Dannenberg, J., Hilmer, T., Duncan, J., Duncan, J.M., Ferrier, B., 2014. An examination of the feasibility of linear deterministic sea wave prediction in multidirectional seas using wave profiling radar: theory, simulation,

and sea trials. J. Atmos. Ocean. Technol. 31 (7), 1601–1614. URL. http://journals.ametsoc.org/doi/abs/10.1175/JTECH-D-13-00170.1.

Belmont, M.R., Horwood, J.M.K., Thurley, R.W.F., Baker, J., 2006. Filters for linear sea-wave prediction. Ocean. Eng. 33 (17), 2332–2351. URL. http://www.sciencedirect.com/science/article/pii/S0029801806000205.

Blondel, E., Bonnefoy, F., Ferrant, P., 2010. Deterministic non-linear wave prediction using probe data. Ocean. Eng. 37 (10), 913–926. URL. http://www.sciencedirect.com/science/article/pii/S0029801810000661.

Blondel-Couprie, E., 2009. Reconstruction et prévision déterministe de houle à partir de données mesurées. phdthesis. Ecole Centrale de Nantes (ECN), Nantes, France. URL. https://tel.archives-ouvertes.fr/tel-00449343.

Blondel-Couprie, E., Bonnefoy, F., Ferrant, P., 2013. Experimental validation of non-linear deterministic prediction schemes for long-crested waves. Ocean. Eng. 58, 284–292. URL. http://www.sciencedirect.com/science/article/pii/S0029801812003988.

Blondel-Couprie, E., Naaijen, P., 2012. Reconstruction and prediction of short-crested seas based on the application of a 3D-FFT on synthetic waves: Part 2 — prediction. In: Volume 5: Ocean Engineering; CFD and VIV. ASME, Rio de Janeiro, Brazil, p. 55. URL. http://proceedings.asmedigitalcollection.asme.org/proceeding.aspx?doi=10.1115/OMAE2012-83096.

Bonnefoy, F., Ducrozet, G., Le Touzé, D., Ferrant, P., 2010. Time domain simulation of nonlinear water waves using spectral methods. In: Advances in Numerical Simulation of Nonlinear Water Waves. Vol. 11 of Advances in Coastal and Ocean Engineering. World Scientific, pp. 129–164. URL. https://www.worldscientific.com/doi/abs/10.1142/9789812836502_0004.

Bonnefoy, F., Le Touzé, D., Ferrant, P., 2006. A fully-spectral 3D time-domain model for second-order simulation of wavetank experiments. Part A: formulation, implementation and numerical properties. Appl. Ocean Res. 28 (1), 33–43. URL. http://www.sciencedirect.com/science/article/pii/S0141118706000551.

Booij, N., Ris, R.C., Holthuijsen, L.H., 1999. A third-generation wave model for coastal regions: 1. Model description and validation. J. Geophys. Res.: Oceans 104 (C4), 7649–7666. URL. https://agupubs.onlinelibrary.wiley.com/doi/abs/10.1029/98JC02622.

Choi, Y.M., Gouin, M., Ducrozet, G., Bouscasse, B., Ferrant, P., 2017. Grid2Grid : HOS Wrapper Program for CFD Solvers. URL. http://arxiv.org/abs/1801.00026.

Desmars, N., Perignon, Y., Ducrozet, G., Guérin, C.-A., Grilli, S.T., Ferrant, P., 2018. Phase-resolved reconstruction algorithm and deterministic prediction of nonlinear ocean waves from spatio-temporal optical measurements. In: Proceedings of the 37th International Conference on Ocean, Offshore and Arctic Engineering, OMAE2018. Ocean Engineering. American Society of Mechanical Engineers, Madrid, Spain. https://doi.org/10.1115/OMAE2018-78367. V07BT06A054. URL.

Dommermuth, D., 2000. The initialization of nonlinear waves using an adjustment scheme. Wave Motion 32 (4), 307–317. URL. http://www.sciencedirect.com/science/article/pii/S0165212500000470.

Dommermuth, D.G., Yue, D.K.P., 1987. A high-order spectral method for the study of nonlinear gravity waves. J. Fluid Mech. 184, 267–288 publisher: Cambridge University Press. URL. https://www.cambridge.org/core/journals/journal-of-fluid-mechanics/article/highorder-spectral-method-for-the-study-of-nonlinear-gravity-waves/89E8FAC1EA7D3FB5F70D37ED4A2B2054.

Ducrozet, G., Bonnefoy, F., Le Touzé, D., Ferrant, P., 2005. Development of a fully nonlinear water wave simulator based on Higher Order Spectral theory. In: Proc. 20th Int. Workshop on Water Waves and Floating Bodies. Longyearbayen, Norway, p. 4.

Ducrozet, G., Bonnefoy, F., Le Touzé, D., Ferrant, P., 2006. Implementation and validation of nonlinear wavemaker models in a HOS numerical wave tank. Int. J. Offshore Polar Eng. 16, 03. https://www.onepetro.org/journal-paper/ISOPE-06-16-3-161. URL.

Ducrozet, G., Bonnefoy, F., Le Touzé, D., Ferrant, P., 2007. 3-D HOS simulations of extreme waves in open seas. Nat. Hazards Earth Syst. Sci. 7 (1), 109–122. URL. https://www.nat-hazards-earth-syst-sci.net/7/109/2007/.

Ducrozet, G., Bonnefoy, F., Le Touzé, D., Ferrant, P., 2012. A modified High-Order Spectral method for wavemaker modeling in a numerical wave tank. Eur. J. Mech. B Fluid 34, 19–34. URL. http://www.sciencedirect.com/science/article/pii/S0997754612000180.

Ducrozet, G., Bonnefoy, F., Le Touzé, D., Ferrant, P., 2016. HOS-ocean: open-source solver for nonlinear waves in open ocean based on High-Order Spectral method. Comput. Phys. Commun. 203, 245–254. URL. http://www.sciencedirect.com/science/article/pii/S0010465516300327.

Fucile, F., Bulian, G., Lugni, C., 2018. A probabilistic approach for the quantification of prediction error in deterministic phase-resolved wave forecasting. Ocean. Eng. 163, 718–736. URL. http://www.sciencedirect.com/science/article/pii/S0029801818305900.

Huchet, M., 2017. Etat de l'art des technologies capables de mesurer la vitesse du fluide en milieu océanique. Rapport interne, Ecole Centrale de Nantes (ECN), Nantes, France.

Huchet, M., Gilloteaux, J.-C., Babarit, A., Ducrozet, G., Perignon, Y., Ferrant, P., 2018. Prédiction déterministe de houle par mesure du profil de vitesse horizontale. In: 16èmes Journées de l'Hydrodynamique. Marseille, France. URL. https://hal.archives-ouvertes.fr/hal-02013239.

Klein, M., Dudek, M., Clauss, G.F., Ehlers, S., Behrendt, J., Hoffmann, N., Onorato, M., 2020. On the deterministic prediction of water waves. Fluid 5 (1), 9. URL. https://www.mdpi.com/2311-5521/5/1/9.

Klein, M., Dudek, M., Clauss, G.F., Hoffmann, N., Behrendt, J., Ehlers, S., 2019. Systematic experimental validation of high-order spectral method for deterministic wave prediction. In: Proceedings of the 38th International Conference on Ocean, Offshore and Arctic Engineering, OMAE2019. American Society of Mechanical Engineers Digital Collection, Glasgow, Scotland, UK, p. 10. URL. https://asmedigitalcollection.asme.org/OMAE/proceedings/OMAE2019/58851/V07BT06A056/1067933.

Köllisch, N., Behrendt, J., Klein, M., Hoffmann, N., 2018. Nonlinear real time prediction of ocean surface waves. Ocean. Eng. 157, 387–400. URL. https://linkinghub.elsevier.com/retrieve/pii/S0029801818303184.

Kosleck, S., 2013. Prediction of wave structure interaction by advanced wave field forecast. In: Executive Summary of the PhD Thesis with the Same Title. Ph.D. thesis.

Law, Y.Z., Santo, H., Lim, K.Y., Chan, E.S., 2020. Deterministic wave prediction for unidirectional sea-states in real-time using Artificial Neural Network. Ocean. Eng. 195, 106722. URL. http://www.sciencedirect.com/science/article/pii/S0029801819308339.

Longuet-Higgins, M.S., Phillips, O.M., 1962. Phase velocity effects in tertiary wave interactions. J. Fluid Mech. 12 (3), 333–336 publisher: Cambridge University Press. URL. https://www.cambridge.org/core/journals/journal-of-fluid-mechanics/article/phase-velocity-effects-in-tertiary-wave-interactions/4D285B2A5B28B862839C0463830F204A.

Lu, Y., Lueck, R.G., 1999. Using a broadband ADCP in a tidal channel. Part I: mean flow and shear. J. Atmos. Ocean. Technol. 16 (11), 1556–1567. URL. https://journals.ametsoc.org/doi/full/10.1175/1520-0426%281999%29016%3C1556%3AUABAIA%3E2.0.CO%3B2.

Morris, E.L., Zienkiewicz, H.K., Belmont, M.R., 1998. Short term forecasting of the sea surface shape. Int. Shipbuild. Prog. 45 (444), 383–400.

Naaijen, P., Huijsmans, R., 2008. Real time wave forecasting for real time ship motion predictions. In: Volume 4: Ocean Engineering; Offshore Renewable Energy. ASME, pp. 607–614. Estoril, Portugal. http://proceedings.asmedigitalcollection.asme.org/proceeding.aspx?articleid=1633634. URL.

Naaijen, P., Trulsen, K., Blondel-Couprie, E., 2014a. Limits to the extent of the spatio-temporal domain for deterministic wave prediction. Int. Shipbuild. Prog. 61 (3–4), 203–223. URL. http://content.iospress.com/articles/international-shipbuilding-progress/isp113.

Naaijen, P., van Dijk, R.R.T., Huijsmans, R.H.M., El-Mouhandiz, A.A., 2009. Real time estimation of ship motions in short crested seas. In: Volume 4: Ocean Engineering; Ocean Renewable Energy. Ocean Space Utilization, Parts A and B. ASME, Honolulu, Hawaii, USA, pp. 243–255. URL. http://proceedings.asmedigitalcollection.asme.org/proceeding.aspx?articleid=1624129.

Naaijen, P., Wijaya, A.P., 2014b. Phase resolved wave prediction from synthetic radar images. In: Proceedings of the 33rd International Conference on Ocean, Offshore and Arctic Engineering, OMAE2014. Ocean Engineering. ASME, San Francisco, California, USA. https://doi.org/10.1115/OMAE2014-23470. V08AT06A045. URL.

Nguyen, H.-N., Sabiron, G., Tona, P., Kramer, M.M., Sanchez, E.V., 2016. Experimental validation of a nonlinear MPC strategy for a wave energy converter prototype. In: Volume 6: Ocean Space Utilization; Ocean Renewable Energy. American Society of Mechanical Engineers, Busan, South Korea. V006T09A019–V006T09A019. URL. http://proceedings.asmedigitalcollection.asme.org/proceeding.aspx?doi=10.1115/OMAE2016-54455.

Nortek, A., 2017. Signature principles of operation. URL. https://www.nortekgroup.com/assets/software/N3015-011-SignaturePrinciples.pdf.

Nouguier, F., Guérin, C.-A., Chapron, B., 2009. "Choppy wave" model for nonlinear gravity waves. J. Geophys. Res.: Oceans 114 (C9). URL. https://agupubs.onlinelibrary.wiley.com/doi/pdf/10.1029/2008JC004984. https://agupubs.onlinelibrary.wiley.com/doi/abs/10.1029/2008JC004984.

Qi, Y., Wu, G., Liu, Y., Kim, M.-H., Yue, D.K.P., 2018a. Nonlinear phase-resolved reconstruction of irregular water waves. J. Fluid Mech. 838, 544–572. URL. https://www.cambridge.org/core/product/identifier/S0022112017009041/type/journal_article.

Qi, Y., Wu, G., Liu, Y., Yue, D.K.P., 2018b. Predictable zone for phase-resolved reconstruction and forecast of irregular waves. Wave Motion 77, 195–213. URL. http://www.sciencedirect.com/science/article/pii/S0165212517301518.

Richter, M., Magana, M.E., Sawodny, O., Brekken, T.K.A., 2013. Nonlinear model predictive control of a point Absorber wave energy converter. IEEE Transactions on Sustainable Energy 4 (1), 118–126.

Sergeeva, A., Slunyaev, A., 2013. Natural hazards and earth system sciences. Rogue waves 14.

Simanesew, A., Trulsen, K., Krogstad, H.E., Nieto Borge, J.C., 2017. Surface wave predictions in weakly nonlinear directional seas. Appl. Ocean Res. 65, 79–89. URL. http://www.sciencedirect.com/science/article/pii/S0141118716303613.

Terray, E., Brumley, B., Strong, B., 1999. Measuring waves and currents with an upward-looking ADCP. In: Proceedings of the IEEE Sixth Working Conference on Current Measurement (Cat. No.99CH36331), pp. 66–71.

The WAMDI Group, 1988. The WAM model—a third generation ocean wave prediction model. J. Phys. Oceanogr. 18 (12), 1775–1810. American Meteorological Society. URL. https://journals.ametsoc.org/jpo/article/18/12/1775/7537/The-WAM-Model-A-Third-Generation-Ocean-Wave.

Toffoli, A., Gramstad, O., Trulsen, K., Monbaliu, J., Bitner-Gregersen, E., Onorato, M., 2010. Evolution of weakly nonlinear random directional waves: laboratory experiments and numerical simulations. J. Fluid Mech. 664, 313–336. URL. https://www.cambridge.org/core/journals/journal-of-fluid-mechanics/article/evolution-of-weakly-nonlinear-random-directional-waves-laboratory-experiments-and-numerical-simulations/0B1A3E4C72712BCC69C9BEF3CC79E3EA.

Toffoli, A., Onorato, M., Bitner-Gregersen, E., Osborne, A.R., Babanin, A.V., 2008. Surface gravity waves from direct numerical simulations of the Euler equations: a comparison with second-order theory. Ocean. Eng. 35 (3), 367–379. URL. http://www.sciencedirect.com/science/article/pii/S0029801807002168.

Tolman, H.L., 2009. User manual and system documentation of WAVEWATCH III TM version 3.14. Technical note. MMAB Contribution 276, 220.

Trulsen, K., 2005. Spatial evolution of water surface waves. In: Proc. Ocean Wave Measurement and Analysis. Fifth International Symposium WAVES, pp. 1–10.

Trulsen, K., Stansberg, C.T., 2001. Spatial Evolution of Water Surface Waves: Numerical Simulation and Experiment of Bichromatic Waves. International Society of Offshore and Polar Engineers. URL. https://www.onepetro.org/conference-paper/ISOPE-I-01-247.

West, B.J., Brueckner, K.A., Janda, R.S., Milder, D.M., Milton, R.L., 1987. A new numerical method for surface hydrodynamics. J. Geophys. Res.: Oceans 92 (C11), 11803–11824. URL. https://agupubs.onlinelibrary.wiley.com/doi/abs/10.1029/JC092iC11p11803.

Wu, G., 2004. Direct Simulation and Deterministic Prediction of Large-Scale Nonlinear Ocean Wave-Field. Thesis,. Massachusetts Institute of Technology. URL. http://dspace.mit.edu/handle/1721.1/33450.

Wu, G., Liu, Y., Yue, D.K.P., 2000. Numerical Reconstruction of Nonlinear Irregular Wave-Field Using Single or Multiple Probe Data. Faculty of Engineering, Tel-Aviv University, Tel-Aviv, Israel, oCLC, 51380882.

Xiao, W., Liu, Y., Wu, G., Yue, D.K.P., 2013. Rogue wave occurrence and dynamics by direct simulations of nonlinear wave-field evolution. J. Fluid Mech. 720, 357–392 publisher: Cambridge University Press. URL. https://www.cambridge.org/core/journals/journal-of-fluid-mechanics/article/rogue-wave-occurrence-and-dynamics-by-direct-simulations-of-nonlinear-wavefield-evolution/535CEB14DAEDF44F684538695D73E5E5.

Yoon, S., Kim, J., Choi, W., 2016. An explicit data assimilation scheme for a nonlinear wave prediction model based on a pseudo-spectral method. IEEE J. Ocean. Eng. 41 (1), 112–122.

Zakharov, V.E., 1968. Stability of periodic waves of finite amplitude on the surface of a deep fluid. J. Appl. Mech. Tech. Phys. 9 (2), 190–194. https://doi.org/10.1007/BF00913182. URL.

Zhang, H., Ducrozet, G., Klein, M., Guedes Soares, C., 2017. An experimental and numerical study on breather solutions for surface waves in the intermediate water depth. Ocean. Eng. 133, 262–270. URL. http://www.sciencedirect.com/science/article/pii/S0029801817300458.

Zhang, J., Yang, J., Wen, J., Prislin, I., Hong, K., 1999. Deterministic wave model for short-crested ocean waves: Part I. Theory and numerical scheme. Appl. Ocean Res. 21 (4), 167–188. URL. http://www.sciencedirect.com/science/article/pii/S0141118799000115.